Macromolecules

ARTICLE

pubs.acs.org/Macromolecules

Effects of Intermolecular Hydrogen Bondings on Isothermal Crystallization Behavior of Polymer Blends of Cellulose Acetate Butyrate and Poly(3-hydroxybutyrate)

Nattaporn Suttiwijitpukdee,[†] Harumi Sato,[*,†] Jianming Zhang,[‡] and Takeji Hashimoto[†,§]

[†]Department of Chemistry, School of Science and Technology, and Research Center for Environment Friendly Polymers, Kwansei-Gakuin University, Sanda 669-1337, Japan

[‡]Key Laboratory of Rubber-plastics, Ministry of Education, Qingdao University of Science and Technology, Qingdao City 266042, People's Republic of China

ABSTRACT: Effects of hydrogen bondings (*HBs*) on the isothermal crystallization kinetics and mechanisms of poly(3-hydroxybutyrate) (PHB) in neat PHB and its blends with cellulose acetate butyrate (CAB), amorphous melts at the crystallization temperature, were investigated by using time-resolved Fourier transform infrared spectroscopy (FTIR). The FTIR investigation focused on the characteristic bands of PHB in the crystalline phase and in the amorphous phase. The results revealed the following pieces of evidence. (1) The crystallization of PHB in both neat PHB and PHB/CAB blends commonly involves a multistep process: (i) transformation from amorphous melts to an intermediated structure between amorphous and crystals (process (b1) shown above), (ii) from the intermediate structure to crystals without intramolecular HBs (*intra*) (b2), and (iii) finally to crystals with *intra* (b3). (2) These transformations sequentially occur with increasing time. More specifically, the transformations (ii) and (iii) dominantly occur respectively in the primary and secondary crystallization process in both neat PHB and the blends. The Avrami analysis revealed that (3) the crystallization in both neat PHB and the blends involves essentially the same nucleation and growth mechanism, as evidenced by almost the same value of the Avrami exponent n; however (4) the crystallization rate constant k_A, also determined from the Avrami analysis, is strikingly reduced by blending CAB (see the k_A value for the PHB/HCAB blend in the text), which is attributed to physical cross-links formed by intermolecular *HBs* between PHB and CAB in addition to molecular entanglements.

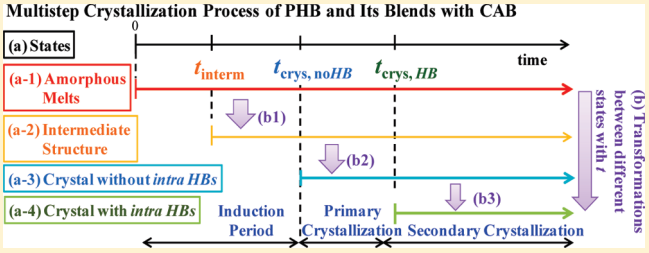

1. INTRODUCTION

1.1. Objectives of This Work. In this work we aim to explore effects of intermolecular (*inter*) and intramolecular (*intra*) hydrogen bondings (*HBs*) on crystallization kinetics and mechanism of poly(3-hydroxybutyrate) (PHB) and cellulose acetate butyrate (CAB), which are biodegradable, by means of time-resolved Fourier transform spectroscopy (FTIR). The work was motivated by the fact that there have been almost no reports along this line, despite significances of the exploration to control structure and properties of ecologically important materials, as will be detailed below. The work is believed to be important with respect to a basic physical science from a viewpoint of ordering of molecular systems involving *inter HBs* and *intra HBs* and their exchanges. We investigated time evolutions of the bands assigned to crystalline phase ("crystalline bands") and to amorphous phase ("amorphous bands") to clarify the crystallization kinetics and mechanism of neat PHB and its blends with CABs.

1.2. Backgrounds of This Work. Polymer blending with natural polymers has attracted a great attention for the development of new polymeric materials, since the properties of natural polymers can be significantly improved by blending with the counter polymers.[1−3] Poly(3-hydroxybutyrate) (PHB) is a bio-synthesized semicrystalline polyester which holds a high potential as a environment-friendly biodegradable thermoplastic.[4−7] PHB has a high melting point, a high degree of crystallinity, and a low glass transition temperature. However, it has some problems on processablility[8,9] because it is thermally unstable at temperatures above its melting point (T_m), specifically due to the β-elimination reaction.[10] Thus, blending of PHB with suitable polymers may offer an improved processability at lower temperatures and an opportunity to obtain better products with improved mechanical and thermal properties.

Cellulose derivatives are an intriguing polymer component to be blended with PHB, since they can be obtained from cellulose materials that are abundant in nature. Cellulose esters exhibit a fairly high glass transition temperature (T_g), good clarity, high flexural, and tensile strengths. Moreover, they are also potentially biodegradable.[11−15] Blends of PHB and cellulose esters have been proved to improve the mechanical toughness of PHB.[16] Recently, cellulose acetate butyrate (CAB), a widely used cellulose derivative, has been extensively investigated for improving the elongation at break of PHB copolymers.[17]

Received: February 16, 2011
Revised: March 28, 2011
Published: April 08, 2011

In the PHB/CAB blends, investigations of the crystallization kinetics are very important because the kinetics influences their crystalline superstructures and degree of crystallinity developed under given processing conditions, and hence their physical properties. So far, the miscibility, crystallization, and phase structure of PHB/CAB blends have been explored by many research groups.[18−23] For example, El-Shafee et al.[22] studied the miscibility, crystallization, and morphology of the PHB and CAB blends by using differential scanning calorimetry (DSC), polarized optical microscopy, and small-angle X-ray scattering (SAXS). They indicated that the blends of PHB/CAB in the melt states are miscible and that the spherulites growth rates of PHB are remarkably reduced in the blends. Park et al. have reported that the orientation behavior of PHB crystals upon drawing the blends depends on the blend composition by using polarized FTIR, wide-angle X-ray diffraction (WAXD), and SAXS; *c*-axis orientation will be changed to *a*-axis orientation with increasing the CAB content in the blends.[23]

Along the line described above, we also have been conducting a series of investigations of the crystal structure and crystallization behavior of PHB in PHB/CAB blends as a function of temperature and the blend composition by using FTIR and WAXD.[24] We have found that there are *inter HBs* −C═O···H−O− between the C═O groups of PHB and the O−H groups of CAB (designated hereafter as "*inter*"), *intra HBs* within CAB (designated hereafter as "*intra* CAB"), and weak *intra HBs* within PHB crystals (i.e., *HBs* of −C═O···H−C− between the C═O groups and one of the C−H groups of CH_3, designated hereafter "*intra* PHB").[25−28] This *intra HBs* of −C═O···H−C− stabilize the chain folding in the lamellar structure of PHB.[25−28] Therefore, it is very interesting to investigate these *HBs* during the crystallization process of PHB in PHB/CAB blends. The physical cross-links formed in PHB and CAB chains in the blends due to *inter* have been proposed to reduce mutual diffusivities of the chains and hence to reduce the crystallization rate and crystallinity of PHB under given crystallization conditions.[24]

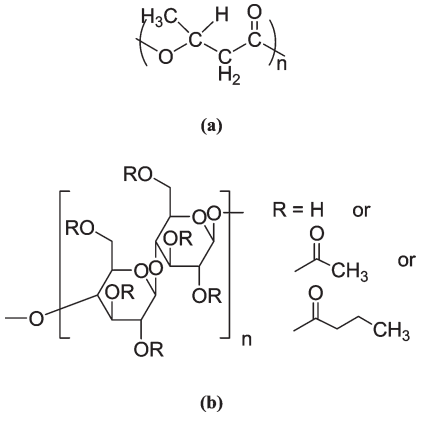

Figure 1. Chemical structures of (a) poly(3-hydroxybutyrate) (PHB) and (b) cellulose acetate butyrate (CAB).

1.3. Special Characteristics of the Two Blends Studied in This Work. One can change the chemical structure of CAB by changing the substituent groups R of its monomeric unit as shown in Figure 1b. CAB's molecular weight also can be changed (e.g., from 70 000 to 12 000 as shown in Table 1). In general, the chemical structure and the molecular weight of CAB give important effects on both crystallization kinetics and resulting morphology. However, these effects have not yet been fully explored. Therefore, in the present study, we aim to investigate these effects on the isothermal crystallization kinetics of PHB/CAB blend systems by selecting two kinds of CAB specimens, designated hereafter as HCAB and LCAB, for a given PHB specimen (see Table 1).

Here it is important to note that the two kinds of CABs selected in this work have the following special characteristics: HCAB has a larger molecular weight (M_n) and larger number of OH groups per single chains (N_{OH}) than LCAB (Table 1). The larger M_n causes the smaller self-diffusivity, D_s, of HCAB compared with that of LCAB. Hence, PHB in the PHB/HCAB blend has a smaller mutual diffusivity, D_m, than PHB in the PHB/LCAB blend. Moreover, the large number of N_{OH} in HCAB cause a large number of *inter*, which acts as physical cross-links between PHB and CAB. This effect of N_{OH} in turn brings about the same effect on D_m as the effect of M_n on D_m: D_m for PHB/HCAB is smaller than D_m for PHB/LCAB. Consequently, in these two blends, the effects of the molecular weight and the effects of the chemical structure are strongly coupled and cooperatively influence the crystallization kinetics in the same direction, giving rise to an extremely large difference in the crystallization rate, as will be clarified later in the sections 3.2, 3.3, and 4.1−4.5.

2. EXPERIMENTAL SECTION

2.1. Materials and Sample Preparation. A PHB (number-average molecular weight, $M_n = 2.9 \times 10^5$) and two kinds of CABs, high-molecular weight CAB (HCAB, $M_n = 7.0 \times 10^4$) and low-molecular weight CAB (LCAB, $M_n = 1.2 \times 10^4$), were purchased from Sigma-Aldrich Co., Ltd., and used as received. Figure 1 shows the chemical structure of PHB (a) and CAB (b). The molecular weight and the compositions of the substituent groups in the monomeric unit of each CAB sample are summarized in Table 1. Concerning potentialities of the blends for forming *inter*, it is important to note the fact that the average number of OH groups per single CAB chain, N_{OH}, for HCAB (N_{OH} = 75.3) is much higher than that for LCAB (N_{OH} = 8.9). The average number of C═O groups in PHB is $2.9 \times 10^5/86.1 = 3368$. The PHB used is semicrystalline below melting temperature T_m (∼172 °C), while the CABs used are totally amorphous.

PHB and CABs were dissolved into a homogeneous solution in chloroform at 80 °C in which the total polymer concentration was 1 wt %. The solution was cast on KBr windows used for FTIR measurements to prepare thin films with the thickness of ∼10 μm. After a majority of the solvent had evaporated, the films were placed under vacuum at 60 °C for

Table 1. Molecular Characteristics of the CAB Samples Used in the Present Study

CAB	M_n	acetyl (mol %)	butyryl (mol %)	hydroxyl (mol %)	M_u	N_{OH}[a]	$N_{C=O,CAB}$[b]	$N_{OH}/N_{C-O,CAB}$
HCAB	70 000	34.3	54.2	11.5	639.1	75.3	582	0.13
LCAB	12 000	43.7	48.6	7.7	650.7	8.9	106	0.085

[a] Average number of OH groups per single CAB chain: $N_{OH} = 6(M_n/M_u)f_{OH}$, where M_u is the average molecular weight of the monomeric unit of CAB and f_{OH} is mole fraction of OH groups in the monomeric unit (0.115 for HCAB and 0.077 for LCAB). [b] Average number of C═O groups per single CAB chain: $N_{C=O,CAB} = 6(M_n/M_u)f_{C=O}$, where $f_{C=O}$ is mole fraction of C═O groups (0.885 for HCAB and 0.923 for LCAB).

16 h to completely remove the residual solvent. The film specimens thus prepared are designated hereafter as as-prepared samples.

2.2. Time-Resolved Measurements of FTIR. Time-resolved FTIR spectra from 4000 to 650 cm^{-1} were collected in situ during the isothermal crystallization on a Thermo Nicolet Magna 6700 FTIR spectrometer equipped with a mercury cadmium telluride (MCT) detector. The normal transmission mode was applied to the FTIR measurements. Before the measurements, the as-prepared neat PHB as well as blends of PHB/HCAB and PHB/LCAB were melted at 190 °C and maintained for 1 min to erase any thermal history built in the as-prepared samples, and then they were cooled down to the isothermal crystallization temperature, T_c, at 117 °C with a cooling rate of 40 °C/min. At T_c = 117 °C, only PHB can be crystallized, while HCAB and LCAB are in amorphous melt. Throughout this work, the time t = 0 is defined at the time when the sample's temperature reach T_c = 117 °C. The FTIR spectra were recorded with 1 min interval in situ during the isothermal crystallization process. To obtain the data with an acceptable signal-to-noise ratio, 32 scans were accumulated for a signal averaging with a 2 cm^{-1} resolution. Temperature of the specimens was controlled by a Linkam controller THMS 600 (Linkam Scientific Instruments Ltd., UK).

2.3. Polarized Optical Microscopy. Evolutions of internal crystalline superstructures of the specimens during the isothermal crystallization process were investigated by using the same specimens and the temperature enclosure and controller as those used for the time-resolved FTIR experiments under polarized optical microscopy.

3. RESULTS

3.1. Composition-Dependent Variation of the Characteristic IR Bands Due to the C═O Stretching Mode at Melts. Figure 2a shows FTIR spectra and their second derivatives in the 1800−1700 cm^{-1} region of neat PHB, HCAB, and their blends with weight fraction of PHB (w_{PHB}) = 0.8 and 0.5 at 190 °C. Figure 2b presents the corresponding spectra of the PHB/LCAB blend system. As can be seen in Figure 2, neat PHB yields one broad band at 1740 cm^{-1}, which is assigned to the "free" amorphous ν(C═O) band[26−28] (designated hereafter as *free* C═O PHB). This indicates that the PHB lamellar crystals completely melt at 190 °C. Although, it is difficult to identify various bands associated with the ν(C═O) band of neat CAB due to a severe overlapping of the bands, the two bands appear at 1758 and 1745 cm^{-1} for HCAB and LCAB in the second-derivative spectra. These two bands may be attributed to the free ν(C═O) band of CAB in slightly different environments (force fields) (designated hereafter as *free* C═O CAB).

The PHB/HCAB blend with w_{PHB} = 0.5 exhibited clearly a new band at 1738 cm^{-1} in the second-derivative spectra. Considering the fact that the ν(C═O) bands at ∼1758 and ∼1745 cm^{-1} in the blend with w_{PHB} = 0.5 existed at the positions similar to those of neat CAB, the new band at 1738 cm^{-1} can be assigned to *inter*, i.e., *HBs* between C═O groups of PHB and OH groups of HCAB C═O···H−O . We interpreted that *inter* causes the *free* C═O PHB at 1740 cm^{-1} shift to a lower wavenumber. The band at 1738 cm^{-1} cannot be clearly discerned in the second derivative spectra for the PHB/HCAB blend with w_{PHB} = 0.8 because of a smaller amount of HCAB and hence a smaller population of *inter* compared with the PHB/HCAB blend with w_{PHB} = 0.5. However, we believe that this band exists for the blend with w_{PHB} = 0.8 as will be detailed below in conjunction with Figure 4. Compared with HCAB, the population of *inter* in the blend with LCAB appears to be relatively small as evidenced by the fact that the band at 1738 cm^{-1} could not be clearly discerned. As shown in Table 1, the average number of the OH groups per single CAB chain, N_{OH}, is less for LCAB than that for HCAB by an order of magnitude. Therefore, it is reasonable to expect

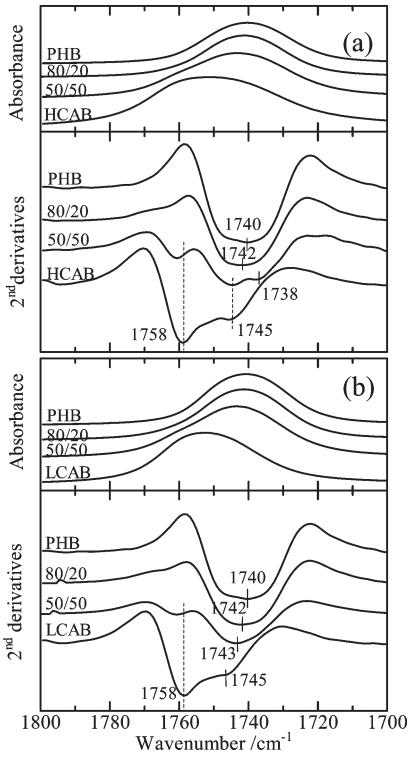

Figure 2. FTIR spectra in the C═O stretching region from 1800 to 1700 cm^{-1} of neat PHB, HCAB, and PHB/HCAB blends (a) and neat PHB, LCAB, and PHB/LCAB blends (b) at 190 °C. Normalized absorbance spectra are shown in the top panels, and their corresponding second-derivative spectra are shown in the bottom panels.

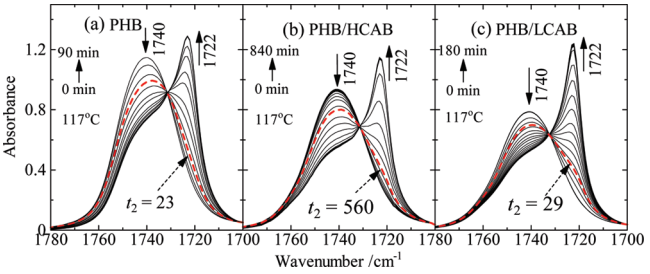

Figure 3. Time-resolved FTIR spectra in the region of 1780−1700 cm^{-1} collected during the isothermal crystallization processes of neat PHB (a), the PHB/HCAB blend (80/20) (b), and PHB/LCAB blend (80/20) (c) at 117 °C. t_2 is the critical time determined from Figure 10.

that there are a larger numbers of *inter* in PHB/HCAB than in PHB/LCAB blends.

Such difference should affect the isothermal crystallization behavior of PHB in the blend systems because *inter* influences the average number of physical cross-linking points incorporated per single PHB chain. For elucidating this point, the isothermal crystallization behavior of PHB/CABs blend with w_{PHB} = 0.8 was investigated in the present study. However, the crystallization of PHB in the blends with w_{PHB} = 0.5 was so slow that the isothermal crystallization behavior was studied only for the blends with w_{PHB} = 0.8.

3.2. Evolutions of the C═O Stretching Bands of PHB during Isothermal Crystallization. Figures 3a−c show time-resolved FTIR spectra in the 1780−1700 cm^{-1} region measured

dx.doi.org/10.1021/ma200365e |*Macromolecules* 2011, 44, 3467–3477

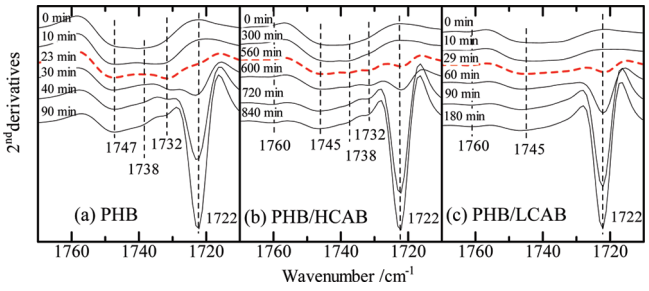

Figure 4. Second-derivative spectra corresponding to the spectra shown in Figure 3.

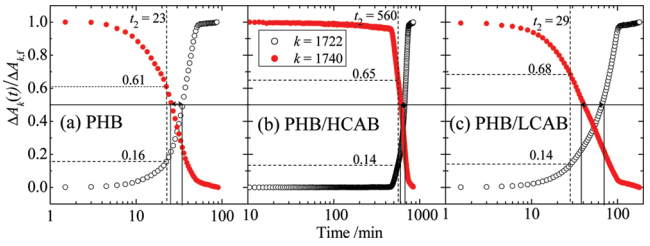

Figure 5. Normalized difference spectral intensity $[\Delta A_k(t)/\Delta A_{k,f}]$ of the crystalline band at 1722 cm^{-1} (○) and the amorphous band at 1740 cm^{-1} (●) for neat PHB (a), PHB/HCAB (b), and PHB/LCAB (c) blends with $w_{PHB} = 0.8$ as a function of crystallization time at 117 °C. The time t_2 has the same meaning as that in Figure 3.

in the isothermal crystallization process of neat PHB, and PHB/HCAB, and PHB/LCAB blends with w_{PHB} = 0.8 at 117 °C, respectively. Each part of the figure shows a gradual but monotonic decrease of *free* C═O PHB at 1740 cm^{-1} of amorphous PHB with a concurrent, gradual, and monotonic increase of *intra* PHB (see the definition in section 1.2) at 1722 cm^{-1} of PHB crystals with the crystallization time. Note that the time $t = 0$ for the isothermal crystallization process was defined already in section 2.2. The meaning of the red broken line drawn at the critical time t_2 in this figure as well as in Figure 4 will be described later in conjunction with Figure 10. It is noted that the blend of PHB/LCAB finishes the crystallization in a shorter period than the blend of PHB/HCAB, which will be quantitatively analyzed and discussed later in section 4.5. It is also noted that the time changes in the characteristic *free* C═O CAB bands at 1758 and 1745 cm^{-1} cannot be identified in the spectra shown in Figure 3 because of a severe overlapping with *free* C═O PHB at 1740 cm^{-1} and of a small value of $w_{CAB} \equiv 1 - w_{PHB}$ in the blends. To resolve their time evolutions, the corresponding second-derivative spectra are plotted in Figure 4.

In Figures 4b,c, the two *free* C═O CAB bands at 1760 and 1745 cm^{-1}, which arise from the different molecular environments, keep their wavenumber almost constant independent of time in the whole crystallization process for both PHB/HCAB and PHB/LCAB. Interestingly, during the crystallization process, a new band clearly appears at 1732 cm^{-1} in a parallel with the evolution of the 1722 cm^{-1} band for PHB and PHB/HCAB after 10 and 480 min, respectively. As for the origin of this band, there are two possibilities: One is attributed to the ν(C═O) band of PHB, and the other is attributed to the ν(C═O) band of CAB. Since CAB always exists in the amorphous state, there is no change in the characteristic bands at 1760 and 1745 cm^{-1} during the crystallization process of PHB. If the new band at 1732 cm^{-1} were due to the ν(C═O) band of CAB, this band also would not change with time during the crystallization. Therefore, the new band at 1732 cm^{-1} can be attributed to the ν(C═O) band of PHB.

As described above in Figure 3, the amorphous and crystalline bands of PHB locate at 1740 and 1722 cm^{-1}, respectively. Then, what kind of a physical state of PHB is the new band at 1732 cm^{-1} related to? The previous reports assigned this band to a less ordered crystal[29] or an "intermediate structure"[30] between crystalline and amorphous state with respect to the spatial molecular arrangements by adopting the concept proposed for the first time by Strobl,[31] though its detailed local structure for PHB was not yet identified.[29,30] We also support this assignment. It should be noted that this band is not discernible for PHB/LCAB, although the reason is not understood at this moment.

The second-derivative spectra in Figure 4a suggest existence of the band at 1738 cm^{-1} for neat PHB also. Although this band may not be clearly discerned in Figure 4a, it is clearly discernible in the original spectra. Moreover, this band for neat PHB was confirmed by 2D correlation analysis.[30] For neat PHB, an overlap of the bands at 1738 and 1747 cm^{-1} seems to show a broad absorbance peak at ~1740 cm^{-1} shown in Figure 3. A close observation of the time evolution of the two bands at 1738 and 1732 cm^{-1} appears to indicate that the two bands roughly change oppositely: when the former band becomes clear, the latter band become less clear and vice versa. Consequently, we assign the band at 1738 cm^{-1} to the amorphous band having conformations different from another amorphous band at 1747 cm^{-1}, which is consistent with our previous report.[30] The band at 1738 cm^{-1} for the PHB/HCAB blend with w_{PHB} = 0.8 at 117 °C in Figure 4b appears to be clearer than that at 190 °C in Figure 2a. This is probably because the population of *inter* is higher at 117 °C than at 190 °C.

Figure 5 shows time evolutions of the difference spectra $\Delta A_k(t)$ normalized with respect to $\Delta A_{k,f}$, $\Delta A_k(t)/\Delta A_{k,f}$ (k = 1722 or 1740 cm^{-1}), during the isothermal crystallization for neat PHB (a), PHB/HCAB (b), and PHB/LCAB (c). The difference spectrum was defined by $\Delta A_k(t) \equiv A_k(t) - A_{k,f}$ and $\Delta A_{k,f} \equiv A_k(t=0) - A_{k,f}$ with $A_k(t)$ and $A_{k,f}$ being the absorbance at k cm^{-1} at time t and that after the completion of the crystallization, respectively. Naturally, $\Delta A_k(t)/\Delta A_{k,f}$ for the amorphous band at 1740 cm^{-1} decrease with t, while that for the crystalline band at 1722 cm^{-1} increases with t, commonly for all the systems. However, it is intriguing to note that a half-time $(t_{1/2})_k$ for the time evolution is shorter at k = 1740 cm^{-1} than at k = 1722 cm^{-1} commonly for all the systems. This piece of evidence reveals itself that amorphous PHB chains are transformed into "the intermediate structure" prior to formation of the crystals responsible for the evolution of A_{1722} in the case of neat PHB. In the case of PHB/HCAB and PHB/LCAB, the amorphous chains are transformed not only into the intermediate structure but also into those incorporated into *inter* before the transformation into the crystals with *intra HBs*. Moreover, the difference of $(t_{1/2})_k$ between k = 1722 and k = 1740, defined as $\Delta t_{1/2}$, as well as $(t_{1/2})_k$ themselves increases in the order of PHB neat (9 min), PHB/LCAB (26 min), and PHB/HCAB (60 min), as listed in Table 2. This trend will be discussed later in section 4.5. The set of the data on $(t_{1/2})_k$ with k = 1229, 1184, and 825/895 cm^{-1} in Table 2 will be also discussed later in section 4.2. The data on t_2 and $\Delta A_k(t)/\Delta A_{k,f}$ at $t = t_2$ also will be discussed later in section 4.1.

3.3. Spectral Evolutions in the C−H Bending and C−O−C Stretching Regions of PHB during the Isothermal Crystallization. Figures 6a,b present spectra of PHB/HCAB and PHB/LCAB in the region of 1400−1100 cm^{-1}, respectively, which are

Table 2. Half-Time $(t_{1/2})_k$ for the Spectral Change of $\Delta A_k(t)/\Delta A_{k,f}$ in the Isothermal Crystallization Process[a]

	$(t_{1/2})_k$/min[b]			$(t_{1/2})_k$/min			$(t_{1/2})_k$/min[e]	
specimen	k = 1722 cm^{-1} (crystal)	k = 1740 cm^{-1} (amorphous)	$\Delta t_{1/2}$[c]	k = 1229 cm^{-1} (crystal)	k = 1184 cm^{-1} (amorphous)	$\Delta t_{1/2}$[d]	k = 825/895 cm^{-1} (crystal)	$\Delta t_{1/2}$[f]
PHB	35	26	9	32	27	5	30	3
PHB/HCAB	668	608	60	633	602	31	620	18
PHB/LCAB	66	41	26	44	32	12	36	4

[a] The induction period t_1 for the spectral change was not subtracted to evaluate $(t_{1/2})_k$. [b] Estimated from the data shown in Figure 5. [c] $\Delta t_{1/2} \equiv (t_{1/2})_{1722} - (t_{1/2})_{1740}$. [d] $\Delta t_{1/2} \equiv (t_{1/2})_{1229} - (t_{1/2})_{1184}$. [e] $(t_{1/2})_{825} \cong (t_{1/2})_{895}$. [f] $\Delta t_{1/2} \equiv (t_{1/2})_{825/895} - (t_{1/2})_{1184}$.

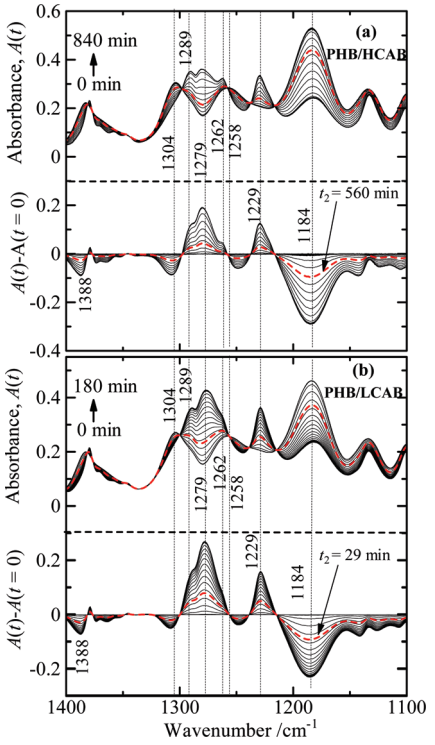

Figure 6. Time-resolved FTIR spectra (top panel) and their corresponding difference spectra (bottom panel) in the region of 1400−1100 cm^{-1} of the PHB/HCAB blend (80/20) (a) and PHB/LCAB blend (80/20) (b) in the isothermal crystallizations at 117 °C. The time t_2 has the same meaning as that in Figure 3.

very sensitive to the conformation and packing of the PHB chain in crystals. In parts a and b, the top panel shows the absorbance $A(t)$ at a given time t during the crystallization, while the bottom panel represents the time change in the difference spectra $\Delta A(t) \equiv A(t) - A(t=0)$. Remarkable spectral changes can be readily seen around 1304, 1279, 1258, 1229, and 1184 cm^{-1} for both blends during the crystallization process. The band at 1184 cm^{-1} can be assigned to the amorphous band due to the asymmetric stretching vibration of the C−O−C group in the PHB.[30] The bands at 1304 and 1258 cm^{-1} can be assigned to the amorphous band due to the C−H bending of PHB chains in the helical conformation.[26,27] These were transformed and split into the four sharp peaks at 1289, 1279, 1262, and 1229 cm^{-1}, when the crystallization occurs. Moreover, the corresponding difference spectra, $\Delta A(t)$, clearly demonstrate that the intensities of these crystalline bands increase accompanied by the decrease of the amorphous bands at 1304 and 1258 cm^{-1} in the crystallization process. The spectral changes in the split peaks at 1289,

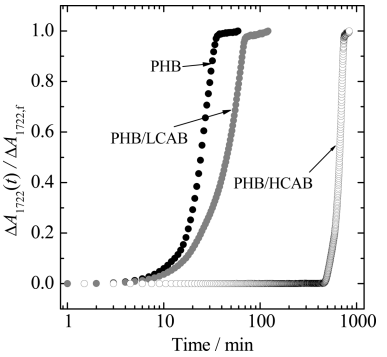

Figure 7. Normalized difference spectral intensity of the crystalline band at 1722 cm^{-1} as a function of crystallization time.

1279, 1262, and 1229 cm^{-1} observed for neat PHB were almost identical to those found for both PHB/HCAB and PHB/LCAB blends, and hence the spectral changes in neat PHB were not included in the text. It should be also noted that, though its intensity is weak, the crystalline band at 1229 cm^{-1} appears to be relatively well separated from other bands compared with the crystalline bands at 1289, 1279, and 1262 cm^{-1}. The red broken lines at t_2 = 560 and 29 min will be discussed later in conjunction with Figure 10.

4. ANALYSES AND DISCUSSION

4.1. Analyses and Discussion of Crystallization Kinetics Based on the C=O Stretching Bands of PHB. The time evolution of the band at 1722 cm^{-1}, assigned to the ν(C=O) band from PHB crystals having the *intra HBs*,[26−28] is anticipated to capture the crystallization process of PHB in the neat PHB and the PHB/CAB blends. Thus, the normalized difference spectra at 1722 cm^{-1}, $\Delta A_{1722}(t)/\Delta A_{1722,f}$, were presented in Figure 7 as a function of the crystallization time t for the neat PHB and the PHB/HCAB and PHB/LCAB blends at w_{PHB} = 0.8. At this moment let us assume for simplicity that $\Delta A_{1722}(t) \propto X_c(t)$ and $\Delta A_{1722,f} \propto X_f$, where $X_c(t)$ and $X_{c,f}$ is the crystallinity at time t and that after the completion of the crystallization, respectively. Then we get

$$\Delta A_{1722}(t)/\Delta A_{1722,f} = X_c(t)/X_{c,f} \quad (1)$$

so that the normalized spectral change with time given by eq 1 reflects the change of the normalized crystallinity $X_c(t)/X_{c,f}$ with time. Figure 7 indicates that the crystallization of PHB/LCAB and PHB/HCAB completes at ~100 and ~750 min, respectively, much later than the neat PHB (~90 min). Obviously, both of the blends show a large induction period, t_{ind}, than neat PHB.

The kinetics of crystallization can be analyzed on the basis of the Avrami's equation:[32,33]

dx.doi.org/10.1021/ma200365e |Macromolecules 2011, 44, 3467–3477

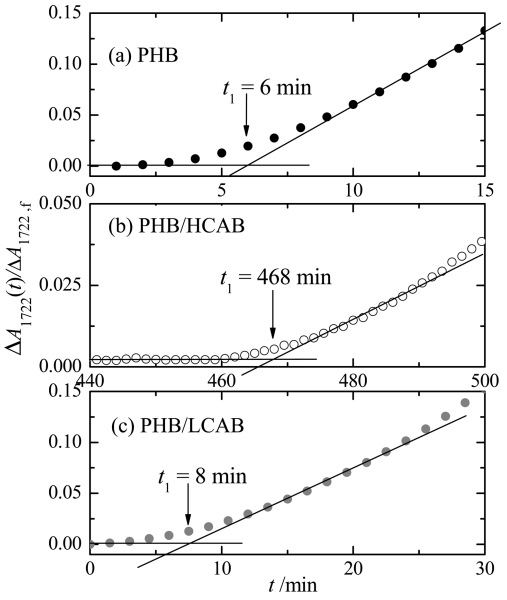

Figure 8. Determination of the induction time t_1 for the normalized spectral intensity change of the crystalline band at 1722 cm^{-1} of the neat PHB (a), PHB/LCAB blend (b), and PHB/HCAB blend (c).

$$X_c(t)/X_{c,f} = 1 - \exp(-k_A t^n) \quad (2)$$

Here k_A is the crystallization rate constant, which depends on nucleation mechanism (homogeneous vs heterogeneous), linear growth rate of crystals G, the growth habit (dimensionality) of the growing crystals and nucleation rate $\dot{N}$ (in the case of homogeneous nucleation), or the number of heterogeneous nuclei $\overline{N}$ in the case of heterogeneous nucleation. On the other hand, the Avrami exponent n depends on the growth habit and the nucleation mechanism. From eq 2, we obtain

$$\ln\{-\ln[1 - (X_c(t)/X_{c,f})]\} = \ln k_A + n \ln t \quad (3)$$

Equation 3 provides a conventional method to evaluate the Avrami constants k_A and n from the time evolution of $\Delta A_{1722}(t)/\Delta A_{1722,f}$ on the basis of the assumption given by eq 1. The time t in eqs 2 and 3 refers to the time elapsed after $X_c(t)$ starts to increase from zero and corresponds to $(t - t_1)$ in our definition of t (see section 2.2), where t_1 is the induction time for the onset of the crystallization. It is important to note that the determination of $t = 0$ in eqs 2 and 3 or t_1 in $(t - t_1)$ in our definition for the Avrami plot significantly influences the values of k_A and n obtained from the plot.

Figure 8 shows the time evolution of $\Delta A_{1722}(t)/\Delta A_{1722,f}$ focused on only in the early stage of the whole spectral change with time shown in Figure 7. As a first trial, we assumed that t_1 can be evaluated as an intercept of the two straight lines as shown in the figure. The value t_1 is assumed to be an induction period for the spectral change as well as that for an inception of the crystallization process which gives rise to the increase of $X_c(t)$ from zero. Actually, we confirmed the fact that spherulites are nucleated and grown only at $t > t_1$ for PHB, PHB/HCAB, and PHB/LCAB, as will be shown later in Figure 11. Consequently, the assumption made above seems reasonable.

Then the normalized spectral changes (shown by symbols) are replotted in Figure 9a against the effective time $(t - t_1)$ appropriate for the Avrami analysis with eq 2 or 3. The figure

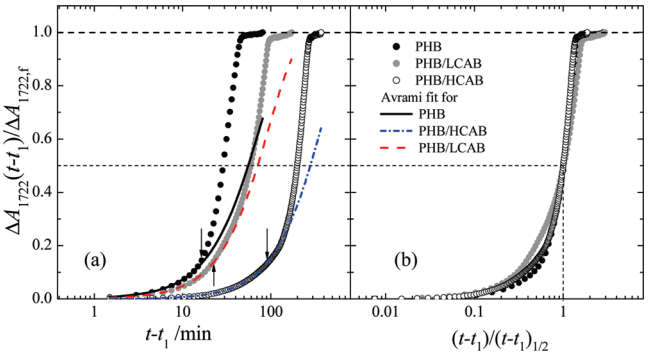

Figure 9. Changes of the normalized difference spectral intensity of the crystalline band at 1722 cm^{-1} with $t - t_1$ (a) and $(t - t_1)/(t - t_1)_{1/2}$ (b). The black line, red broken line, and blue dash-dotted line are Avrami fit shown in Figure 10 for PHB, PHB/HCAB, and PHB/LCAB, respectively.

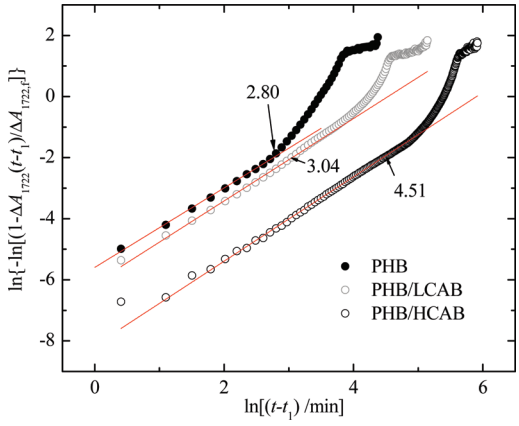

Figure 10. Avrami plots for the crystalline band at 1722 cm^{-1} of neat PHB (●), PHB/HCAB blend (○), and PHB/LCAB blend (○). The arrows indicate the critical times t_2's, satisfying $\ln[t_2 - t_1]/\text{min}] = 2.80$, 3.04, and 4.51 for PHB, PHB/LCAB, and PHB/HCAB for the onset of the deviations of the data points from the Avrami plot.

clearly demonstrates the increase of the crystallization half-time, $(t - t_1)_{1/2}$, and the time span $(t - t_1)_f$ between t_1 and the time t_f for the completion of the crystallization in the order of neat PHB (29 and 74 min), PHB/LCAB (59 and 164 min), and PHB/HCAB (200 and 350 min), respectively. The solid, broken, and dash-dotted lines in Figure 9a will be discussed below in conjunction with Figure 10. Figure 9b shows the reduced spectral changes against the reduced time, $(t - t_1)/(t - t_1)_{1/2}$, for the same three systems. The reduced curves are not universal, indicating that the crystallization mechanism and kinetics as observed by the spectral changes are different for the three systems.

The nonuniversality of the reduced curves shown in Figure 9b further motivated us to analyze them by means of the Avrami plots, the results of which are shown in Figure 10. The results revealed that the early stage of the spectral change can be well approximated by a straight line as given by eq 3 for each of the systems. The Avrami parameters thus determined from the 1722 cm^{-1} band are summarized in the row of 1722 cm^{-1} in Table 3 for PHB, PHB/HCAB, and PHB/LCAB together with t_1 and $(t - t_1)_{1/2}$. The results shown in Figure 10 indicate the upward deviations of the data in the late stage at $t \geq t_2$ from the straight lines as well, where t_2's are the critical time for the onset of the deviations as indicated by the arrows in Figure 10.

dx.doi.org/10.1021/ma200365e |*Macromolecules* 2011, 44, 3467–3477

Table 3. Characteristic Parameters for the Isothermal Crystallization As Evaluated by Using the Avrami Plots and Choosing the Induction Period t_1 for the Time Evolution of the Various Crystalline Bands

				Avrami constants	
sample	observed band (cm^{-1})	induction time t_1 (min)	half-time $(t - t_1)_{1/2}$ (min)	n	$k_A \times 10^{-3}$ min^{-n}
PHB	1722	6	29	1.3	3.7
	1229	6	26	1.4	4.2
	825	6	26	1.2	5.6
PHB/HCAB	1722	468	200	1.4	0.29
	1229	473	162	1.3	0.68
	825	471	147	1.4	0.51
PHB/LCAB	1722	8	59	1.4	2.2
	1229	8	36	1.3	6.7
	825	6	30	1.2	9.9

Table 4. Critical Time t_2 and $[\Delta A_k(t=t_2)/\Delta A_{k,f}]$ in the Isothermal Crystallization Process

		$[\Delta A_k(t)/\Delta A_{k,f}]_{at\ t=t_2}$				
sample	t_2[a] (min)	k = 1722	k = 1740	k = 1229	k = 825/895[b]	k = 1184
PHB	23	0.16	0.61	0.23	0.23	0.65
PHB/HCAB	560	0.14	0.65	0.22	0.25	0.67
PHB/LCAB	29	0.14	0.68	0.30	0.38	0.63

[a] The time beyond which the Avrami plot shown in Figure 10 based on k = 1722 cm^{-1} starts to deviate from the straight line. [b] The value $[\Delta A_k(t=t_2)/\Delta A_{k,f}]$ at k = 825 cm^{-1} is equal to that at k = 895 cm^{-1}.

The arrows satisfy $\ln[(t_2 - t_1)]/\text{min}] = 2.80$, 4.51, and 3.04, hence the estimated value of t_2 being 23, 560, and 29 min for PHB, PHB/HCAB, and PHB/LCAB, respectively, as summarized in Table 4.

If the early stage of the spectral change at $t < t_2$, which fits with the straight line in the Avrami plot, corresponds to the primary crystallization process and the late stage at $t > t_2$ corresponds to the secondary crystallization process, we usually expect the downward deviations of the data points in the late stage from the straight lines, simply because the secondary crystallization is usually slower than the primary crystallization. We separately observed the time-resolved growth of crystalline superstructures under polarizing optical microscopy. Figure 11 demonstrates some typical results. We found that the time t_2's were approximately equivalent to those where the spherulites impinge each other to approximately fill a whole sample space commonly for PHB, PHB/HCAB, and PHB/LCAB, as typically shown in parts b and d. Since the behavior of PHB/HCAB with respect to this point was almost the same as that of PHB/LCAB, the data on PHB/HCAB were not included in the figure. We found also the fact that at $t < t_1$ there are no nucleation and growth of spherulites, the nucleation and growth being observed only at $t > t_1$ for all the three systems as typically shown in parts a and c.

Consequently, we confirmed that the early stage and the late stage for these specimens correspond to the primary crystallization process and the secondary crystallization process, respectively. In Figure 9a the black solid line, red broken line, and the blue dash-dotted line correspond to the straight lines shown in Figure 10 for PHB, PHB/LCAB, and PHB/HCAB, respectively. The arrows in Figure 9a correspond to those in Figure 10, and therefore the experimental data in the late stage or the secondary crystallization process reveal the unusual upward deviation from the Avrami fits.

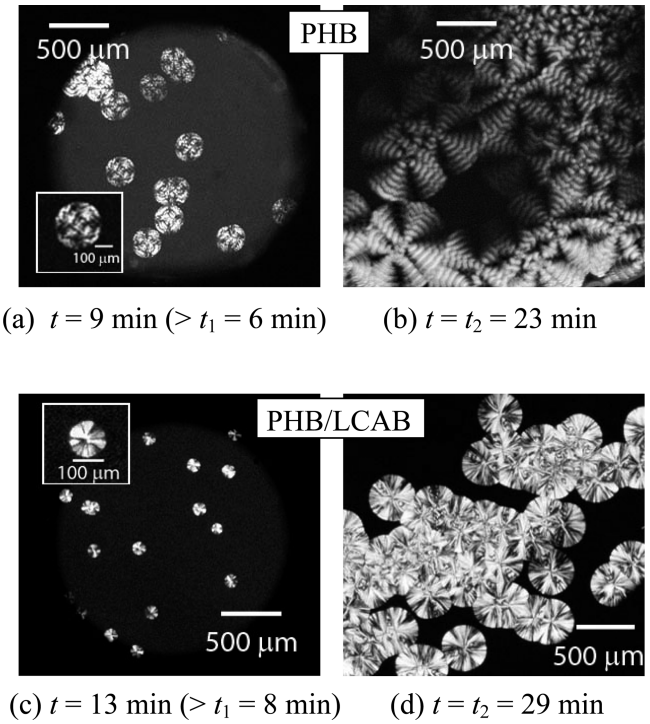

Figure 11. Polarized optical micrographs of PHB at t = 9 min (>t_1 = 6 min) (a) and t_2 = 23 min (b) and of PHB/LCAB at t = 13 min (>t_1 = 8 min) (c) and t_2 = 29 min (d), which were obtained during the isothermal crystallization process at 117 °C. The POM images at $t < t_1$ did not show no spherulites at all for all the specimens, so that the images were not shown.

Thus, it is quite striking to discover the upward deviation of the experimental data in the secondary crystallization process from the Avrami fit in Figures 9 and 10. We think it is crucial to elucidate a physical origin of the upward deviations. The FTIR spectra or the second-derivative spectra at t_2 were highlighted by the red broken line in Figures 3 and 4 for the ν(C═O) band and in Figure 6 for the C−H bending and C−O−C stretching band. We can find that the primary crystallization process at $t_1 \leq t \leq t_2$ is the one where the peak at 1722 cm^{-1} is not well developed in the original spectra and the second-derivative spectra. The difference spectra at 1229 and 1184 cm^{-1} in Figure 6 show only a weak maximum and minimum, respectively. Thus, the primary crystallization process in these systems corresponds to only an early stage of the spectral change of the ν(C═O) band or of the C−H bending and C−O−C asymmetric stretching bands. We believe that a further analysis of the spectral change is crucial for a deeper insights into the mechanisms of the crystallization process in these systems.

4.2. Analyses and Discussion of Crystallization Kinetics Based on the C−H Bending and C−O−C Stretching Bands of PHB. Up to this stage we analyzed the isothermal crystallization process as observed by the ν(C═O) band of PHB. We have conducted similar analyses on the C−H bending and ν(C−O−C) bands of PHB as listed in items 1 and 2 below:

Scheme 1. Multistep Crystallization Process of PHB in Neat PHB and PHB/CAB Blends[a]

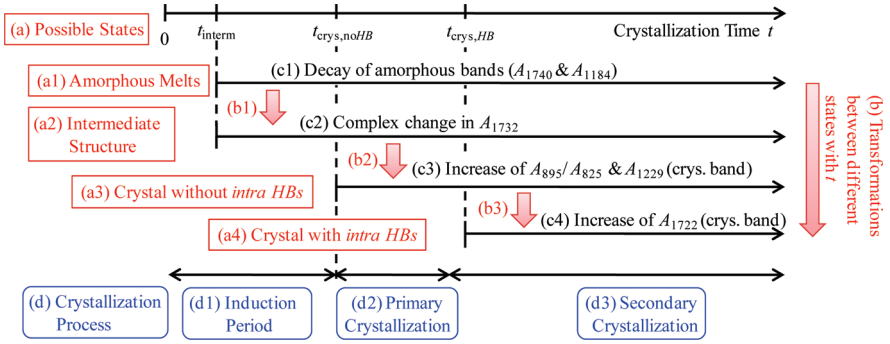

[a] The scheme shows (a) possible states of PHB chains [from (a1) to (a4)], (b) transformations between the different states with t (b1; amorphous to intermediate structure, b2; intermediate structure to crystals without *intra HBs*, b3; crystals without *intra HBs* to crystals with *intra HBs*), (c) the observed spectral changes with t [from (c1) to (c4)], and (d) various crystallization process [from (d1) to (d3)]. The characteristic times of t_{interm}, $t_{cry,noHB}$, and $t_{cry,HB}$ are the onset times for formation of the intermediate structure, crystals without *intra HBs*, and crystals with *intra HBs*, respectively.

(1) The analyses on the time evolution of the reduced difference spectral intensity $\Delta A_k(t)/\Delta A_{k,f}$ for k = 1229, 1184, 895, and 825 cm^{-1}, in a similar manner as shown in Figure 5 for the ν(C═O) bands. The results are summarized in Table 2 and compared with those for the ν(C═O) bands, though the corresponding plots were not included in the text.

(2) The analyses of the induction period t_1 (in a similar manner as shown in Figure 8 for A_{1722}), the crystallization half-time $(t - t_1)_{1/2}$ (in a similar manner as shown in Figure 9 for A_{1722}), and the Avrami constants by using the Avrami plot (in a manner as shown in Figure 10 for A_{1722}) for the spectral changes in the primary crystallization process. The results are summarized in Tables 3 and 4 and compared with those for the ν(C═O) bands, though the corresponding plots are not shown in the text. The Avrami plots based on A_{1229}, A_{1184}, A_{895}, and A_{825} also showed a good linearity for the primary crystallization process, as good as the plot shown in Figure 10, and showed also the upward deviations of the data points in the secondary crystallization process at $t > t_2$ as shown in Figure 10. Thereby the plots are not included in the text.

The results shown in Table 2 reveal the following pieces of evidence for the isothermal crystallization of PHB. $(t_{1/2})_{k=1184} \cong (t_{1/2})_{k=1740} < (t_{1/2})_{k=1229} \cong (t_{1/2})_{k=825/895}$ (evidence 1). The crystallization half-time as observed by the spectral change of the amorphous band of 1184 cm^{-1} is nearly equal to that of the amorphous band of 1740 cm^{-1}. They are smaller than those as observed by the spectral changes of the crystalline bands of 1229, 895, and 825 cm^{-1} which are nearly equal to one another. These results indicate that (i) the absorbances of these two amorphous bands at 1184 and 1740 cm^{-1} (defined as A_{1184} and A_{1740}, respectively) decay commonly due to a series of events found at $t \geq t_{interm}$ (the onset time for formation of the intermediate structure) as indicated in Scheme 1 [see the spectral change (c1)]: the transformation from amorphous melts (a1) to the intermediate structure (a2) at $t \equiv t_{interm}$ [the process (b1)], then to lamellar crystals without *intra HBs* (a3) at $t \equiv t_{crys,noHB}$ [the process (b2)] and finally to lamellar crystals with *intra HBs* (a4) at $t \equiv t_{crys,HB}$ [the process (b3)] in the order of the increasing crystallization time t. Here the characteristics times $t_{crys,noHB}$ and $t_{crys,HB}$ designate the onset time for formation of crystals without *intra HBs* and the onset time for formation of crystals with *intra HBs*, respectively. The multistep crystallization process which involves the intermediate structure or less ordered crystals is consistent in general with the model proposed by Strobl.[31]

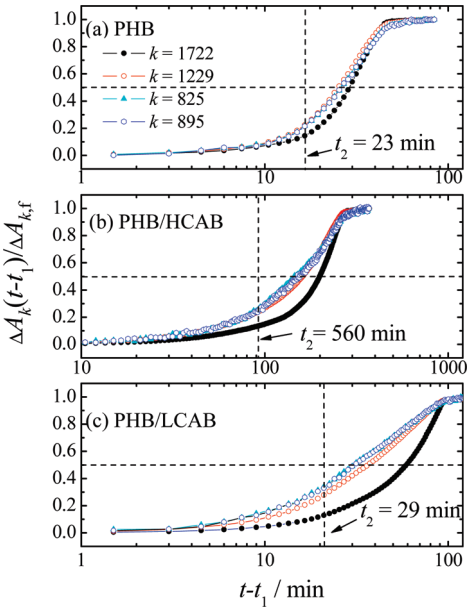

Figure 12. Normalized difference spectral intensity as a function of the crystallization time $(t - t_1)$ for the crystalline bands at 1722, 1229, 895, and 825 cm^{-1}.

The processes (b1) and (b2) respectively increase and decrease A_{1732}, so that its spectral change with t is complex [see the spectral change in (c2) in Scheme 1]. The results also indicate that (ii) the absorbances of these three crystalline bands at 1229, 895, and 825 cm^{-1} (defined as A_{1229}, A_{895}, and A_{825}, respectively) increase commonly due to a series of events occurring at $t \geq t_{crys,noHB}$ [see the spectral change in (c3) in Scheme 1]. The increase of A_{1229}, A_{895}, and A_{825} with t will be explicitly clarified later in conjunction with Figure 12. Interestingly, this experimental result infers that the process (b3) will not decrease A_{1229}, A_{895}, and A_{825}, which in turn elucidates such an important fact that these bands originate not only from crystals without *intra HBs* but also from crystals with *intra HBs*, thereby the process (b3) from (a3) to (a4) hardly giving rise to changes in A_{1229},

dx.doi.org/10.1021/ma200365e |*Macromolecules* 2011, 44, 3467–3477

A_{895}, and A_{825}. The results shown in Table 2 reveal also the fact that $(t_{1/2})_{k=1229} < (t_{1/2})_{k=1722}$ (evidence 2). This indicates that (iii) *intra HBs* are formed at $t > t_{crys,HB}$ within the crystals which are free from *intra HBs* and which have been formed at $t \geq t_{crys,noHB}$ as shown in Scheme 1 [see the spectral change in (c4) and the process (b3)].

In the case of the blends, Table 2 further elucidates the followings, in addition to evidence 1 and evidence 2 as described above for neat PHB: $(t_{1/2})_k$s for the blends are large than $(t_{1/2})_k$s for neat PHB for any one of the given spectra k (evidence 3). Physical significances of this result will be discussed later in section 4.5. Furthermore, the enlarged $(t_{1/2})_k$s for the blends reveal also a trend that $(t_{1/2})_{k=825/895}$ is slightly smaller than $(t_{1/2})_{k=1229}$ (evidence 4). This trend indicates that (iv) the bands at 825 and 895 cm^{-1} may be more sensitive to the intermediate structure than the band at 1229 cm^{-1} and hence starts to increase slightly earlier than $t_{crys,noHB}$ before formation of the crystals free from *intra HBs*, although this trend is not explicitly presented in Scheme 1.

The results summarized in Scheme 1 clearly elucidate the fact that formation of the intermediate structure during the crystallization process can be most clearly recognized by the "apparent change" in A_{1722} crystalline band with time. This is because the band is not affected and buried by the increase of the absorbance due to the lamellar crystallization without *intra HBs* up to the time $t = t_{crys,HB}$ and because the band is expected to contain the contributions of the crystals with *intra HBs* and that of the intermediate structure [compare processes (c2) to (c4) in Scheme 1].

The experimental facts (evidence 1 to evidence 4) found above in conjunction with Table 2 can be confirmed also by Figure 12, which shows the normalized difference spectra $\Delta A_k(t - t_1)/\Delta A_{k,f}$ as a function of the effective crystallization time $(t - t_1)$ after the induction time t_1 for the crystalline bands at 1722, 1229, 895, and 825 cm^{-1}. The figure clearly elucidates that the time evolutions of A_{825} and A_{895} are almost identical and slightly faster than that of A_{1229} for the blends and that the time evolution of A_{1722} is much behind than those of A_{825}, A_{895}, and A_{1229}. The fact that the time evolutions of A_{825}, A_{895}, and A_{1229} are caught up by that of A_{1722} at the long time limit elucidates the fact that A_{825}, A_{895}, and A_{1229} are attributed to not only the crystals without *intra HBs* but also the crystals with *intra HBs*, although the contribution of the crystals without *intra HBs* to these spectra itself decreases with time. The figure elucidates also the fact that the primary crystallization as observed by POM, which completes at t_2, occurs at much earlier stage than the half-times $(t_{1/2})_k$s as observed by the spectral changes and that formation of the crystals with *intra HBs*, and hence the evolution of A_{1722} occurs primarily in the secondary crystallization process at $t > t_2$.

4.3. Discussion about Consequences of Avrami Analyses. Table 3 compares the results obtained from the Avrami's analyses where the analyses done for the amorphous bands of 1740 and 1184 cm^{-1} were excluded, simply because their spectral changes reflect not only the crystal formation but also for formation of the intermediate structure in the case of neat PHB and for formation of *inter* as well in the case of the blends. The induction time t_1 for the spectral change is almost independent of the spectra investigated in this work for both neat PHB and the blends and hence corresponds to $t_{crys,noHB}$ shown in Scheme 1. Almost the same arguments as those given for $(t_{1/2})_k$ in Table 2 can be applied to the crystallization half-time $(t - t_1)_{1/2}$. The Avrami exponent n = 1.3−1.4 is almost independent of the spectrum selected and is the same for neat PHB and the blends. The crystallization rate constant k_A also is independent of the spectrum selected but strikingly depends on the systems: $(k_A)_{PHB/HCAB} \ll (k_A)_{PHB} \cong (k_A)_{PHB/LCAB}$, the trend of which will be discussed later in section 4.5. The physical implications of these Avrami constants n and k_A also will be separately discussed in the next section.

Table 4 shows the time t_2 at the end of the primary crystallization and the values of the normalized difference spectra $F_k(t) \equiv [\Delta A_k(t)/\Delta A_{k,f}]$ at $t = t_2$ for various bands at 1722, 1740, 1229, 1184, and 825/895 cm^{-1} for neat PHB, PHB/HCAB, and PHB/LCAB. The values F_k(t) increase with time for the crystalline bands at 1722, 1229, and 825/895 cm^{-1}, while the value $[1 - F_k(t)]$ increase with time for the amorphous bands at 1740 and 1184 cm^{-1}. These values at $t = t_2$ are related to the progress of the crystallization at the end of the primary crystallization. The time t_2 increases in the order of PHB, PHB/LCAB, and PHB/HCAB, physical significances of which will be discussed later in section 4.5. The fact that $F_{k=1722}(t_2) < F_{k=1229}(t_2) \lesssim F_{k=825/895}(t_2)$ for both neat PHB and the blends elucidates again the fact that formation of the crystals having *intra HBs* occurs after formation of the crystals free from *intra HBs*, as shown in Scheme 1. The fact that $1 - F_{k=1740}(t_2) \cong 1 - F_{k=1184}(t_2) > F_k(t_2)$ for all the crystalline bands (k = 1722, 1229, and 825/895 cm^{-1}) and for neat PHB and the blends elucidates again the fact that spectral changes in the amorphous bands include formation of the intermediate structure prior to the crystallization in the case of neat PHB and formation of the intermediate structure and *inter* in the case of the blends.

4.4. Discussion about Physical Interpretations of Avrami Exponents n = 1.3−1.4. As presented in Table 3, we found that the exponent n was equal to 1.3−1.4, a constant value independent of the samples, neat PHB, and the blends PHB/HCAB and PHB/LCAB. This means that the nucleation mechanism (homogeneous or heterogeneous) and the growth habit of PHB are the same for all the samples. The specific value of n = 1.3−1.4 suggests the following two plausible models.

Model 1. The homogeneous nucleation with one-dimensional growth habit with its growth being controlled by diffusional process predicts the value n given by[34]

$$n = 1.5 \tag{4}$$

On the basis of the same concept, we can derive

$$k_A = (\text{constant}) D^{1/2} k_n \tag{5}$$

where the constant depends on $X_{cs}\rho_s/\rho$ with X_{cs}, ρ_s, and ρ being crystallinity within spherulites, density of spherulites, and density of polymers. In eq 5, D is the diffusion constant of PHB: more specifically, $D = D_s$ for neat PHB and $D = D_m$ for the blends. k_n is the nucleation rate constant.

Model 2. The heterogeneous nucleation with one-dimensional growth habit, which involves sporadic nucleation with specific probability on predetermined nuclei N, predicts the following equation[34]

$$\ln[1 - X_c(t)/X_{c,f}] = -(\text{constant}) G\overline{N} t \tag{6}$$

if vt is large, so that all the predetermined nuclei are activated simultaneously or

$$\ln[1 - X_c(t)/X_{c,f}] = -(\text{constant}) G\overline{N} v t^2 \tag{7}$$

if vt is small, so that the predetermined nuclei are activated at a constant rate ($\overline{N}v = \dot{N}$, the nucleation rate) throughout the

course of the crystallization. Thus, according to this model, n varies between 1 and 2

$$1 \leq n \leq 2 \tag{8}$$

depending on the value vt.[34] k_A accordingly varies between eqs 9 and 10:

$$k_A = (\text{constant})G\overline{N}, \quad \text{if } vt \text{ is large} \tag{9}$$

$$k_A = (\text{constant})G\dot{N}, \quad \text{if } vt \text{ is large} \tag{10}$$

Consequently, the observed exponent n can be accounted for in the context of the one-dimensional growth habit of the crystals according to either model 1 or 2 commonly for neat PHB and for the blends of PHB/HCAB and PHB/LCAB. The small k_A for PHB/HCAB is accounted for on the basis of a small value of $D^{1/2}k_n$ for the case of diffusion-controlled homogeneous nucleation (model 1) or a small value of $G\overline{N}$ or $G\dot{N}$ for the case of the sporadic heterogeneous nucleation (model 2). In all the cases the crystal growth habit is predicted to be one-dimensional: the lamellar growth occurs selectively along a particular direction.

Zhang et al.[30] previously reported $n \sim 2.6$ and 2.5 for the isothermal crystallization of PHB at 129 °C based on the spectral change of A_{825} and A_{1184} with time, respectively. The reported values of n are much larger than those in the present work. The disparity of n in the two experiments may be due partly to differences in mobilities of PHB used (differences in the crystallization temperature and molecular weight) and partly to lack of a rigorous evaluation of the induction time t_1 and subtraction of t_1 from the time t taken from the inception of the isothermal crystallization at T_c in their Avrami analysis.

4.5. Discussion about Comparison of the Crystallization Kinetics of the Two Blends. In order to make a fair comparison of the crystallization kinetics of the two blends PHB/HCAB and PHB/LCAB in reference to that of neat PHB, it is crucial to recall once again the special features of the two blends with respect to M_n and N_{OH} (Table 1), which are pointed out earlier in section 1. Namely, in these two blends, the effects of the molecular weight (M_n) and the chemical structure (N_{OH}) reinforce each other cooperatively in the same direction on the crystallization kinetics via their effects on the mutual diffusivity of PHB. Therefore, the larger M_n and N_{OH} in HCAB bring about a higher physical cross-links via *inter* and higher entanglement couplings, which leads to a greater suppression of the crystallization rate of PHB, compared to the blends with LCAB which have the smaller M_n and N_{OH}.

These features described above account for the differences in the following characteristic parameters among PHB/HCAB, PHB/LCAB, and PHB: the induction period t_1, the crystallization half-time $t_{1/2}$ (the nominal value including t_1) or $(t - t_1)_{1/2}$ (the effective value after the onset of crystallization), the time t_2 for the end of primary crystallization or the onset of the secondary crystallization the time, t_f for the completion of the crystallization, and the crystallization rate constant k_A as determined from the Avrami plot. The experimental results obtained in this work are summarized as follows:

$$(X)_{\text{PHB/HCAB}} \gg (X)_{\text{PHB/LCAB}} > (X)_{\text{PHB}} \tag{11}$$

where X in $(X)_K$ refers to any quantities described above: t_1, $t_{1/2}$, $(t - t_1)_{1/2}$, t_2, t_f, and k_A^{-1}, and the subscript K refers to the relevant systems. These pieces of information are elucidated as follows: t_1 from Figures 8 and 11 as well as Table 3; $t_{1/2}$ or $(t - t_1)_{1/2}$ from Figures 5, 9, and 12 as well as Tables 2 and 3; t_2 from Figures 10 and 12 and Table 4; t_f from Figures 3−5 and 7; and k_A from Table 3. The three specimens showed almost the same Avrami exponent n as discussed already in section 4.4.

Although the special features of HCAB and LCAB discussed above yielded the unique results as summarized in eq 11, they made a decoupling of the effects of the molecular weight and the effects of the chemical structure on the crystallization kinetics difficult. In order to decouple the two effects, one can choose the following CABs: (1) the two CABs having different molecular weights but the same chemical structure for the monomeric units; (2) the two CABs having the same molecular weight but the different chemical structure. The researches based on these PHB/CAB blends are indispensible for creating advanced ecological polymeric materials and deserve future works. Along this line, we think it is intriguing to compare the crystallization kinetics of PHB with that of PHB/LCAB as briefly described below.

PHB and PHB/LCAB with $w_{PHB} = 0.8$ have almost the same glass transition temperature, T_g (−1.7 and −4.9 °C, respectively).[24] Furthermore, LCAB has much lower molecular weight (1.2×10^4) than PHB (2.9×10^5); thus, at $T_c = 117$ °C the mobility of LCAB is larger than that of PHB so that LCAB may act as a plasticizer for PHB, if LCAB and PHB were not able to form *inter*. This effect is expected to make the crystallization rate of PHB in PHB/LCAB faster than neat PHB. However, even the small number of *inter* formed between LCAB and PHB actually slowed down the crystallization rate of PHB in PHB/LCAB compared with that of neat PHB, as found in this work. The result reveals the fact that the effects of the physical cross-links due to *inter* on the crystallization kinetics are much stronger than those due to entanglements.

4.6. Discussion about a Physical Significance of the Upward Deviations of Experimental Data from the Avrami Fit in the Secondary Crystallization Process. We now try to address the problem raised in section 4.1 concerning a physical meaning of the intriguing upward deviations of the experimental data from the Avrami fit which was found in the secondary crystallization process, as shown in Figures 9 and 10 for A_{1722}. It should be noted that the similar deviations were also found for A_{1229}, A_{895}, and A_{825}, as already pointed out in section 4.2. As already summarized in Scheme 1 and Figure 12, the primary crystallization process, which was well characterized by the Avrami equation, involves the transformation from amorphous melts to the crystals without *intra HBs* via the intermediate structure, while the secondary crystallization involves the transformation from the intermediate structure to the crystals without *intra HBs* and then to the crystals with *intra HBs*. The upward deviations then suggest that the latter transformation (from the crystals without to with *intra HBs*) occurs faster than the former transformation. This in turn may suggest that formation of the crystals without *intra HBs* is slower than formation of the crystals with *intra HBs*. This is supported also by the experimental results shown in Figure 12, where A_{1722} is found to increase at much larger rate than A_{1229}, A_{895}, and A_{825} in the secondary crystallization process at $t > t_2$, though it starts to increase at a later time than A_{1229}, A_{895}, and A_{825}.

5. CONCLUSION

Effects of blending of noncrystallizable CAB on the isothermal crystallization of PHB at 117 °C were explored by the time-resolved FTIR analyses of both the crystalline bands and amorphous bands. We discovered that the blending strikingly slows down the crystallization kinetics, as observed by the reduction of the crystallization rate constant k_A determined from

the Avrami plot as well as the prolonged induction time t_1 for the crystallization and the crystallization half-time $(t - t_1)_{1/2}$, without significantly changing the Avrami exponent itself, n = 1.2−1.4, for both neat PHB and the blends. The slowing down of the kinetics was found to be primarily attributed to the physical cross-linkings between PHB chains and CAB chains formed by the intermolecular hydrogen bondings (*HBs*) of PHB−C═O···H−O−CAB. The unaltered n reveals the common crystallization mechanism in the three systems studied: either the homogeneous nucleation with the diffusion-controlled one-dimensional growth habit of the crystals or the heterogeneous nucleation involving sporadic nucleation with specific probability from predetermined nuclei under the one-dimensional growth habit of the crystals.

In both neat PHB and the blends, we discovered the fact that the crystallization involves a series of event as summarized in Scheme 1: first formation of the intermediate structure between crystals and amorphous melts [through process (b1) from state (a1) to (a2)], then lamellae without intramolecular (intra) *HBs* of PHB−C−H···O═C−PHB [through process (b2) from state (a2) to (a3)], and eventually lamellae having *intra HBs* [through process (b3) from state (a3) to (a4)] in the order of the increasing crystallization time. Moreover, we discovered also the fact that the primary crystallization involves primarily formation of the lamellae without *intra HBs*, while formation of *intra HBs* occurs primarily in the secondary crystallization process in the lamellae free from *intra HBs*. Strikingly, our results revealed that this secondary crystallization process occurs at a larger rate than the primary crystallization process, giving rise to the upward deviation from the Avrami fit as found in Figures 9 and 10. This appears to be a specific feature inherent in PHB.

We would like to stress that simultaneous measurements of time evolution of X-ray crystallinity during the course of the isothermal crystallization is crucial to gain a deep insight into the process and mechanisms of the crystallization, particularly the upturn deviation in the time change in the normalized crystallinity from the Avrami fit in the secondary crystallization process, as discovered with the time-resolved FTIR. This is simply because WAXD does not essentially distinguish the crystals without and with *intra HBs* formed during the isothermal crystallization. The simultaneous measurements well deserve future works. The discovery of the multistep crystallization process involving the intermediate structure or the less ordered crystal structure strongly supports in general the model or concept proposed by Strobl.[31]

AUTHOR INFORMATION

Corresponding Author

*E-mail: hsato@kwansei.ac.jp.

Notes

[§]Professor Emeritus, Kyoto University, Kyoto 606-8501, Japan.

ACKNOWLEDGMENT

The authors gratefully acknowledge Prof. Yukihiro Ozaki for encouragements of this work and for many invaluable comments. This work was supported by Grant-in-Aid for Scientific Research (C) from MEXT (No. 20550026, No. 20550197), Grant-in-Aid for Scientific Research on Innovative Areas from MEXT (No. 21106521), and Shiseido Female Researcher Science Grant 2009. This works was supported also by Kwansei-Gakuin University "Special Research" project 2009−2014.

REFERENCES

(1) Utracki, L. A. In *Polymer Blend Handbook*; Kluwer Academic Publishers: Dordrecht, 2002; p 13.
(2) Robeson, L. M. In *Polymer Blend: A Comprehensive Review*; Carl Hanser Verlag: Munich, 2007; p 198.
(3) Yu, L.; Dean, K.; Li, L. *Prog. Polym. Sci.* **2006**, *31*, 576–602.
(4) Doi, Y. In *Microbial Polyesters*; VCH Publishers: New York, 1990.
(5) Doi, Y.; Kitamura, S.; Abe, H. *Macromolecules* **1995**, *28*, 4822–4828.
(6) Vert, M. *Biomacromolecules* **2005**, *6*, 538–546.
(7) Povolo, S.; Casella, S. In *Recent Advances in Biodegradable Polymers and Plastics*; Chiellini, E., Solaro, R., Eds.; Wiley-VCH: Weinheim, 2003; p 1.
(8) Mohanty, A. K.; Misra, M.; Hinrichsen, G. *Macromol. Mater. Eng.* **2000**, *276/277*, 1–24.
(9) Rudnik, E. In *Compostable Polymer Material*, 1st ed.; Elsevier: Amsterdam, 2008; p 21.
(10) Marchessault, R. H.; Yu, G. In *Biopolymers: Polyesters II. Properties and Chemical Synthesis*; Doi, Y., Steinbüchel, A., Eds.; Wiley-VCH: Weinheim, 2003; p 163.
(11) Nishio, Y.; Matsuda, K.; Miyashita, Y.; Kimura, N.; Suzuki, H. *Cellulose* **1997**, *4*, 131–145.
(12) Buchanan, C. M.; Gardner, R. M.; Komarek, R. J. *J. Appl. Polym. Sci.* **1993**, *47*, 1709–1719.
(13) Komarek, R. J.; Gardner, R. M.; Buchanan, C. M.; Gedon, S. *J. Appl. Polym. Sci.* **1993**, *50*, 1739–1746.
(14) Glasser, W. G.; Mccartney, B. K.; Samaranayake, G. *Biotechnol. Prog.* **1994**, *10*, 214–219.
(15) Tachibana, Y.; Giang, N. T. T.; Ninomiya, F.; Funabashi, M.; Kunioka, M. *Polym. Degrad. Stab.* **2010**, *95*, 1406–1413.
(16) Yamaguchi, M.; Arakawa, K. *J. Appl. Polym. Sci.* **2007**, *103*, 3447–3452.
(17) Buchanan, C. M.; Gedon, S. C.; White, A. W.; Wood, M. D. *Macromolecules* **1992**, *25*, 7373–7381.
(18) Lotti, N.; Scandola, M. *Polym. Bull.* **1992**, *29*, 407–413.
(19) Scandola, M.; Ceccorulli, G.; Pizzoli, M. *Macromolecules* **1992**, *25*, 6441–6446.
(20) Ceccoruli, G.; Pizzoli, M.; Scandola, M. *Macromolecules* **1993**, *26*, 6722–6726.
(21) Pizzoli, M.; Scandola, M.; Ceccorulli, G. *Macromolecules* **1994**, *27*, 4755–4761.
(22) El-Shafee, E.; Saad, G. R.; Fahmy, S. M. *Eur. Polym. J.* **2001**, *37*, 2091–2104.
(23) Park, J. W.; Tanaka, T.; Doi, Y.; Iwata, T. *Macromol. Biosci.* **2005**, *5*, 840–852.
(24) Suttiwijitpukdee, N.; Sato, H.; Zhang, J.; Hashimoto, T.; Ozaki, Y. *Polymer* **2011**, *52*, 461–471.
(25) Sato, H.; Nakamura, M.; Padermshoke, A.; Yamaguchi, H.; Terauchi, H.; Sanong, E.; Noda, I.; Ozaki, Y. *Macromolecules* **2004**, *37*, 3763–3769.
(26) Sato, H.; Nakamura, M.; Padermshoke, A.; Hirose, F.; Senda, K.; Noda, I.; Ozaki, Y. *Macromolecules* **2004**, *37*, 7203–7213.
(27) Sato, H.; Dybal, J.; Murakami, R.; Noda, I.; Ozaki, Y. *J. Mol. Struct.* **2005**, *744−747*, 35–46.
(28) Sato, H.; Mori, K.; Murakami, R.; Ando, Y.; Takahashi, I.; Zhang, J.; Terauchi, H.; Hirose, F.; Senda, K.; Tashiro, K.; Noda, I.; Ozaki, Y. *Macromolecules* **2006**, *39*, 1525–1531.
(29) Padermshoke, A.; Katsumoto, Y.; Sato, H.; Ekgasit, S.; Noda, I.; Ozaki, Y. *Spectrochim. Acta, Part A* **2005**, *61*, 541–550.
(30) Zhang, J.; Sato, H.; Noda, I.; Ozaki, Y. *Macromolecules* **2005**, *38*, 4274–4281.
(31) Strobl, G. *Eur. Phys. J. E* **2000**, *3*, 165–183.
(32) Avrami, M. L. *J. Chem. Phys.* **1939**, *7*, 1103–1112.
(33) Avrami, M. L. *J. Chem. Phys.* **1940**, *8*, 212–224.
(34) Mandelkern, L. In *Crystallization of Polymers*; McGraw-Hill: New York, 1964; p 228.